GEOPHYSICS, VOL. 75, NO. 2 (MARCH-APRIL 2010); P. C1–C6, 7 FIGS., 1 TABLE.
10.1190/1.3315861

Assessment of gas-hydrate saturations in the Makran accretionary prism using the offset dependence of seismic amplitudes

Maheswar Ojha[1], Kalachand Sain[1], and Timothy A. Minshull[2]

ABSTRACT

We estimate the saturations of gas hydrate and free gas based on measurements of seismic-reflection amplitude variation with offset (AVO) for a bottom-simulating reflector coupled with rock-physics modeling. When we apply the approach to data from a seismic line in the Makran accretionary prism in the Arabian Sea, the results reveal lateral variations of gas-hydrate and free-gas saturations of 4–29% and 1–7.5%, respectively, depending on the rock-physics model used to relate seismic velocity to saturation. Our approach is simple and easy to implement.

INTRODUCTION

Gas hydrates are crystalline solids of methane and water formed at high pressure and low temperature (Kvenvolden, 1998; Sloan, 1998). They have attracted attention because of their widespread occurrence in permafrost and outer continental margins, their potential as a future major energy resource, and their role in climate change and geohazards (Dillon et al., 1991; Paull et al., 1991; Paull and Dillon, 2001; Milkov, 2004; Taylor and Kwan, 2004; Makogon et al., 2007). The identification and quantification of gas hydrates are essential to evaluate their resource potential and to assess their associated environmental hazard.

Gas hydrates can be identified on multichannel marine seismic reflection data by mapping an anomalous bottom-simulating reflector (BSR), which marks the base of the high-pressure and relatively low-temperature zone in which hydrates are stable (Andreassen et al., 1990, Kvenvolden et al., 1993). Seismic reflections from BSRs exhibit a wide range of amplitude variation with offset (AVO) characteristics that depend upon the saturation and distribution of hydrates above and free gas below the BSR (Hyndman and Spence, 1992; Andreassen et al., 1997; Ecker et al., 1998; Yuan et al., 1999; Carcione and Tinivella, 2000).

Hydrates may form part of the pore fill or part of the rock matrix; where present, gas may be distributed uniformly or in patches throughout the pore space (Dvorkin et al., 1999; Helgerud et al., 1999). Uniform and patchy gas distributions yield different AVO behaviors because of velocity dispersion in partially gas-saturated sediments (White, 1975; Lee, 2004). We assume a uniform distribution of free gas below the BSR, although our method can be adopted for patchy saturation. Overpressure in the trapped gas also affects the AVO responses, but its effect is hard to isolate from the effect of gas on P-wave reflection data because both overpressure and free gas can cause low P-wave velocity (Tinivella, 2002).

In the hydrocarbon industry, AVO attributes have gained considerable popularity for predicting lithology and reservoir characteristics (Castagna and Backus, 1993; Castagna and Smith, 1994; Castagna et al., 1998). Several workers (Hyndman and Spence, 1992; Andreassen et al., 1997; Ecker et al., 1998; Yuan et al., 1999; Carcione and Tinivella, 2000; Chen et al., 2007) estimate hydrate and/or gas saturations from BSRs using conventional AVO modeling and various rock-physics models.

Here, we present a simple approach that compares the AVO intercept A and gradient B estimated from the BSR with those values from two gas-hydrate models to quantify the saturations of gas hydrate and free gas across a BSR. For a theoretical calculation of A and B values, we use the Biot-Gassmann theory by Lee (2002) (BGTL) and the effective medium theory (EMT) of Helgerud et al. (1999); in both, hydrates are considered part of the sediment frame. We demonstrate through a field example in the Makran accretionary prism (Minshull et al., 1992; Sain et al., 2000) that a plot of A versus B can be used to detect free gas below the BSR and to quantify the amount of hydrate and gas along a seismic reflection profile.

THEORY

For a plane wave incident at an interface between two semi-infinite isotropic homogeneous elastic half-spaces and for angles of in-

Manuscript received by the Editor 10 July 2009; revised manuscript received 25 October 2009; published online 12 March 2010.
[1]National Geophysical Research Institute, Council of Scientific and Industrial Research, Hyderabad, India. E-mail: maheswar_ojha@yahoo.com; kalachandsain@yahoo.com.
[2]University of Southampton, National Oceanography Centre Southampton, Southampton, U. K. E-mail: tmin@noc.soton.ac.uk.

cidence θ up to ~30°, the P-wave reflection coefficient $R(\theta)$ can be expressed as (Shuey, 1985)

$$R(\theta) \approx A + B \sin^2 \theta, \quad (1)$$

where

$$A = \frac{1}{2}\left(\frac{\Delta V_P}{V_P} + \frac{\Delta \rho}{\rho}\right) \text{ and } B = AA_0 + \frac{\Delta \sigma}{(1-\sigma)^2}. \quad (2)$$

In addition,

$$A_0 = B_0 - 2(1 + B_0)\frac{1-2\sigma}{1-\sigma},$$

$$B_0 = \frac{\frac{\Delta V_P}{V_P}}{\frac{\Delta V_P}{V_P} + \frac{\Delta \rho}{\rho}},$$

$$V_P = \frac{V_{P2} + V_{P1}}{2}, \quad V_S = \frac{V_{S2} + V_{S1}}{2},$$

$$\rho = \frac{\rho_2 + \rho_1}{2}, \quad \sigma = \frac{\sigma_2 + \sigma_1}{2},$$

$$\Delta V_P = (V_{P2} - V_{P1}), \quad \Delta V_S = (V_{S2} - V_{S1}),$$

$$\Delta \rho = (\rho_2 - \rho_1),$$

$$\Delta \sigma = (\sigma_2 - \sigma_1),$$

and

$$\sigma_i = \frac{0.5V_{Pi}^2 - V_{Si}^2}{V_{Pi}^2 - V_{Si}^2}, \quad i = 1,2.$$

The values V_P, V_S, and ρ are the P-wave velocity, S-wave velocity, and density, respectively. Subscripts 1 and 2 represent the parameters of overlying and underlying layers, respectively. Equations 1 and 2 are valid for large negative A for a negative impedance contrast across an interface (Shuey, 1985; Castagna et al., 1998) and to about $A = 0.2$ for a positive impedance contrast (Shuey, 1985).

Table 1. Parameters used in theoretical calculations (from Lee, 2002).

Component	Bulk modulus (GPa)	Shear modulus (GPa)	ρ (g/cm^3)
Quartz	36	45	2.65
Clay	20.9	6.85	2.58
Hydrate	6.41	2.54	0.91
Methane[a]	0.067	—	0.20
Water	2.25	—	1.00

Critical porosity = 36%
Number of grains/contact = 9
[a]From Ghosh and Sain (2008)

To interpret seismic data in terms of hydrate content, one needs to establish a relation between hydrate saturation in sediments and their velocity. Lee et al. (1996) develop a weighted-equation model in which hydrate velocities are a weighted sum of Wyllie's time-average equation (Wyllie et al., 1958) and Wood's equation (Wood, 1941). However, the weighted-equation model is not based on physical principles and requires empirical calibration. The velocities predicted from the cementation theory proposed by Dvorkin and Nur (1996) are much higher than those normally observed in nature (Ecker et al., 1998). Helgerud et al. (1999) introduce an EMT that considers the hydrate as part of the rock frame and successfully apply their approach to P-wave velocity data from site 995 of ODP leg 164 in the Blake Ridge area. Lee (2002) proposes a method based on Biot-Gassmann theory to relate the elastic properties of sediments to those of the matrix and the pore fluid. Several researchers (Chand et al., 2004; Dai et al., 2004) compare various models and find modest variations in the pattern of velocity with hydrate saturation if the same mineralogy and values of elastic constants are assumed.

Here, we use the EMT and BGTL models to calculate A and B for various gas-hydrate and free-gas saturations. In the absence of direct sampling, we assume quartz and clay as mineralogical constituents for the sediment matrix in the Makran (Sain et al., 2000). For a seafloor porosity ϕ_0 of 60% (Fowler et al., 1985) and a compaction constant λ of 1.17 (Minshull and White, 1989), the porosity at the depth of the BSR (~510 m below the seafloor) is calculated as 39% using Athy's law ($\phi(z) = \phi_0 e^{(-z/\lambda)}$).

Other parameters used in our calculation, taken from Lee (2002), are shown in Table 1. The density and bulk modulus of methane are calculated to be 0.2 g/cm^3 and 67 MPa, respectively, at approximately 21°C and 26.34 MPa pressure (Ghosh and Sain, 2008) at BSR depth using Batzle and Wang's relation (1992). We use a background P-wave velocity (in the absence of gas or hydrate) of 2000 m/s obtained from the normal-moveout (NMO) interval velocity (described in the next section) for both rock-physics models at the BSR depth. The velocity and porosity values correspond to a composition of 10% clay and 90% quartz using the EMT model. Assuming the same composition of clay and quartz, the value of consolidation constant m (Lee, 2004) is adjusted to 2.13 in the BGTL model to obtain a background velocity of 2000 m/s at the BSR depth. We use the Biot coefficient $\beta = -68.7421/(1 + e^{(\phi + 0.40635)/0.09425}) + 0.98469$ for unconsolidated marine sediment (Lee, 2002, 2004) in the BGTL model. The P- and S-wave velocities decrease with increasing β at a given porosity. A reasonable value of β can be calculated by least-squares fitting of the observed data for a range of porosities (Lee, 2002).

We first compute the A and B attributes using equation 2 by varying the hydrate saturation from 0% to 80% at 5% intervals for fixed gas saturations of 0%, 1%, 2%, 5%, and 10% below the BSR. Above approximately 10% gas saturation, the P-wave velocity remains almost unchanged. The resulting variations of A as a function of B for 10% ± 5% clay content at 39% porosity and 39% ± 2% porosity at 10% clay content are shown in Figures 1 and 2, respectively, to demonstrate the effects of clay content and porosity. The porosity is more sensitive than the mineralogical composition to the change in A and B values. In A-B space, a hydrate/brine BSR falls in the second quadrant (negative A and positive B) and is treated as a reference model. The A and B values clearly deviate from this reference trend in the presence of gas below the BSR.

FIELD DATA

We compute the AVO attributes from seismic data (Figure 3) that show a clear BSR in the Makran accretionary prism (Minshull et al., 1992; Sain et al., 2000). The data have 24 traces in each common depth point (CDP) with a maximum offset of 2559 m and dominant frequency of approximately 35 Hz. A representative supergather of CDPs 4378 and 4379 is displayed in Figure 4. The BSR reflection coefficients are calculated from the amplitudes of the seafloor reflection, the BSR, and the first multiple of the seafloor reflection using the approach of Warner (1990). The data-processing sequence included a band-pass filter (4-8-50-60 Hz), a spherical-divergence correction $[1/(\text{time} \times \text{velocity}^2)]$, minimum-phase spiking deconvolution, an NMO correction, and trace equalization. The trace-to-trace or very short wavelength variations are assumed to be noise and need to be eliminated. Trace equalization compensates for amplitude variations from abnormal shot strength and receiver coupling. However, it should be applied very cautiously within a long gate time window (e.g., seafloor to first multiple of seafloor) at the end of all processing steps (Ostrander, 1984; Yu, 1985). Hydrophone directivity is corrected using the function of Sheriff and Geldert (1995). No source directivity correction is applied because the source was of limited spatial extent (Sain et al., 2000).

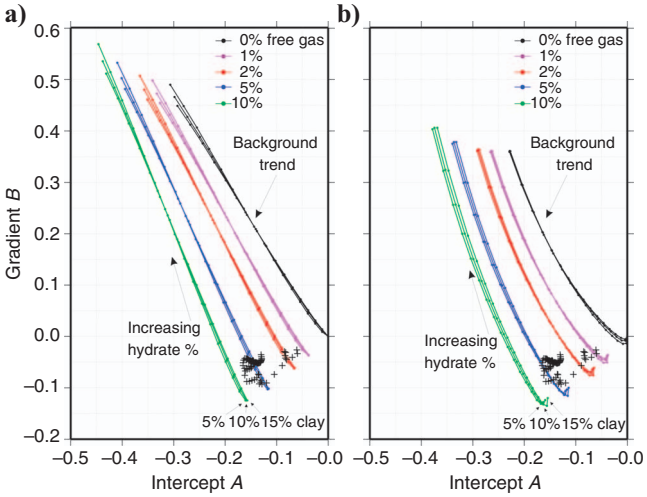

Figure 1. Theoretical crossplots between intercept A and gradient B computed using varying saturations of gas hydrates with several fixed saturations of free gas based on (a) BGTL and (b) EMT models prepared for 10% ± 5% clay content and 39% porosity. Running averages of A and B values (plus signs) estimated for various CDP locations are superimposed.

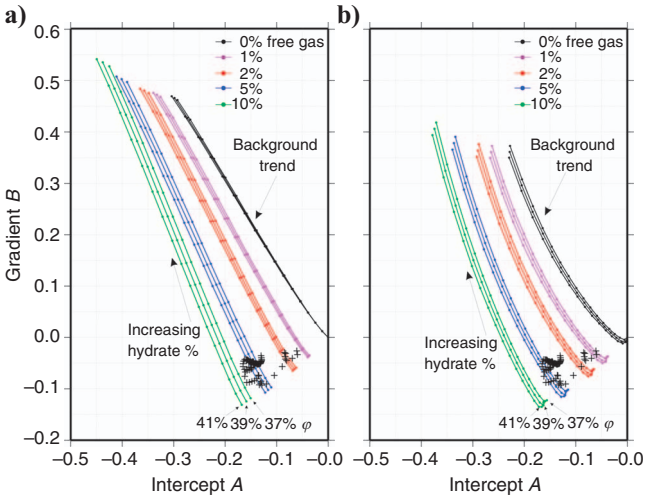

Figure 2. Theoretical crossplots between intercept A and gradient B computed using varying saturations of gas hydrates with several fixed saturations of free gas based on (a) BGTL and (b) EMT models prepared for 39% ± 2% porosity ϕ and 10% clay content. Running averages of A and B values (plus signs) estimated for various CDP locations are superimposed.

The rms amplitudes were picked for a time window of 40–50 ms around the BSR between CDPs 4340 and 4500, where the BSR is strong and relatively flat. The time window was chosen to yield a reliable result despite the change in BSR waveform at CDP 4450. Velocity analysis has been carried out at a 10-CDP interval (225 m). We used vertically smoothed (20 ms), spatially averaged NMO interval velocities (Figure 5) to calculate angles of incidence at the BSR using ray theory. Offsets of up to 1610 m have incidence angles of less than 30° and were considered in the analysis; results differed little if a 25° threshold was taken instead. Reflector depths were obtained by converting the velocity-time function into a velocity-depth function with the Dix formula. A straight line was fit to the averaged interval velocities (Figure 5), which gives a reference velocity of

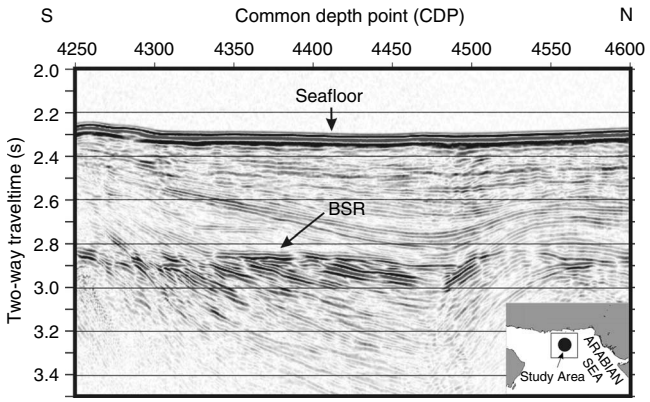

Figure 3. Seismic stacked section along a south-north seismic line in the Makran accretionary prism. Inset shows the study area. The BSR shows crosscutting with dipping strata, opposite polarity with respect to the seafloor reflection, and mimicking of the seafloor topography.

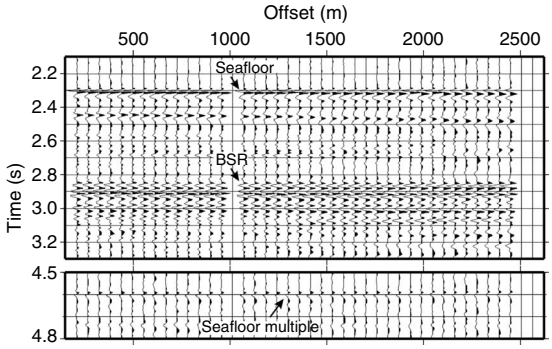

Figure 4. A representative NMO-corrected supergather of CDPs 4378 and 4379, showing reflections from the seafloor, BSR, and first multiple of seafloor reflection. Amplitudes of the multiple and seafloor are used to calculate reflection coefficients of the BSR.

2 km/s at the BSR depth. This velocity was used to calibrate the rock-physics models.

The *A* and *B* values and their associated uncertainties (Figure 6a) were derived by weighted least-squares fitting for each supergather of two consecutive CDPs across the section. A running average of *A* and *B* over CDP location was superimposed on the theoretical nomogram (Figures 1 and 2). The running average removes noise from estimated *A* and *B* values and potentially reveals lateral changes in hydrate and gas content. Figure 6b illustrates the estimated hydrate and gas saturations, with their uncertainties resulting from uncertainties in *A*, *B*, and porosity.

DISCUSSION

The *A* and *B* attributes are a measure of the normal incidence reflection coefficient (P-wave impedance contrast) and change in Poisson's ratio (a function of P- and S-wave velocities), respectively. Hence, the *A*-*B* crossplot coupled with rock-physics modeling is an important tool for estimating gas hydrate and free gas, respectively. The BGTL model shows almost linear trends with hydrate and gas saturations, whereas the EMT model is more nonlinear (Figures 1 and 2). At low hydrate saturations (<10%), the V_P/V_S ratio increases with hydrate saturation because the EMT model predicts little variation in V_S at low hydrate saturation. This complex behavior suggests that it will be difficult to estimate hydrate and gas saturations with the EMT approach when hydrate content is low. The EMT theory predicts higher S-wave velocity than the BGTL theory for any proportion of clay (or quartz) at a specified porosity (for porosity >30%) and vice versa (Lee, 2002; Ojha and Sain, 2008). Thus, the predicted background V_P/V_S ratio for the EMT model is always less than that for the BGTL model, and the EMT model always predicts higher hydrate saturation than that of the BGTL model. The BGTL model is more realistic in the case of quantification from V_P and V_S together.

The uncertainties in hydrate saturation resulting from uncertainties in *A* are small for both models (Figure 6). The maximum uncertainty in hydrate saturation from uncertainties in *B* is ±1.5% for EMT and ±1.0% using BGTL. The corresponding uncertainties in gas saturation for both models are less than ±0.12%. The largest uncertainties come from the EMT-based estimate from error in porosity. Additional uncertainties in estimates of gas saturation come from errors in the assumed density and bulk modulus of the gas, which are dependent on pressure and temperature.

The presence of gas-rich/gas-poor dipping strata, which produce tuning-related highs and lows in amplitude and velocity variations in the gas zone below the BSR (Figure 5), complicate the analysis. By using a supergather of two consecutive CDPs and running an average of *A* and *B* values over a CDP profile, the *A*-*B* crossplot method gives an overall idea of hydrate and gas in the region. AVO modeling of a synthetic seismogram (Figure 7) shows that the crossplot technique works well where the gas layer is thicker than 10 m. As the thickness of the gas layer decreases below this threshold, amplitude increases with offset because of tuning between the top and bottom of the gas layer. In an area where the gas layer thickness is unknown, the crossplot technique can extrapolate interpretation away from a few selected locations where more time-consuming waveform inversion or modeling techniques are applied, as long as the gas layer is greater than 10 m thick. Tuning effects can lead to localized peaks and troughs in *A* and *B* values. By using running means of *A* and *B* values over several CDPs, we can remove most of these artifacts.

The full waveform inversion analysis of two CDP supergathers from the same data set shows that the gas layer is indeed greater than

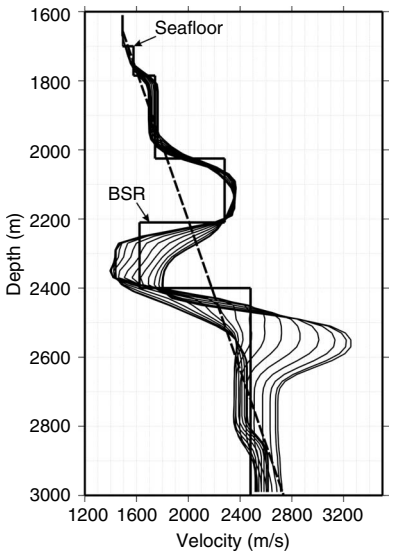

Figure 5. Thin lines show smooth NMO interval velocity functions at 10-CDP intervals between CDPs 4340 and 4500. Thick, solid line shows spatially averaged interval velocity with depth. Dashed line is a straight line fitted to the averaged interval velocity (solid line).

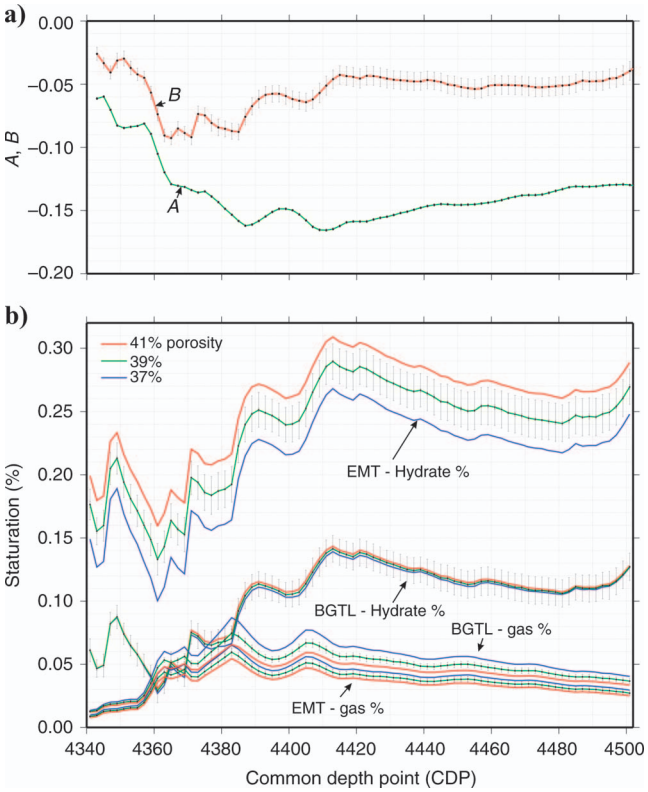

Figure 6. (a) *A* and *B* values (with error bars) against CDPs, estimated based on weighted least-squares fit and then running average for a <30° angle (1610 m offset). (b) Hydrate and gas saturations against CDPs, estimated by EMT and BGTL models at 39% ± 2% porosity and 10% clay content. Error bars are attributable to errors in *A* (small bars) and *B* (large bars) at 39% porosity.

10 m thick (Sain et al., 2000). Using high-frequency (up to 650 Hz) deep-towed multichannel seismic data, Chapman et al. (2002) delineate a thin, 4–8-m negative-velocity-gradient layer at the BSR on the Vancouver Island margin. However, at lower frequencies, as used here, such thin layers may not be resolved, and the BSR commonly appears as a single interface overlying a thick low-velocity zone (e.g., Hyndman and Spence, 1992; Andreassen et al., 1997; Ecker et al., 1998; Yuan et al., 1999; Carcione and Tinivella, 2000).

Gas hydrates may be distributed in concentrations that are laterally and vertically variable, controlled by heterogeneities in lithology, permeability, and methane transport (Ruppel and Kinoshita, 2000; Trehu et al., 2004; Riedel et al., 2006; Collett et al., 2008; Malinverno et al., 2008). An identifiable reflector is always needed to apply an AVO technique such as the *A*-*B* crossplot; in the case of gas-hydrate exploration, the reflector is the BSR. The crossplot technique can be used as an effective tool on a regional scale to assess the gas hydrate and free-gas saturation at the BSR.

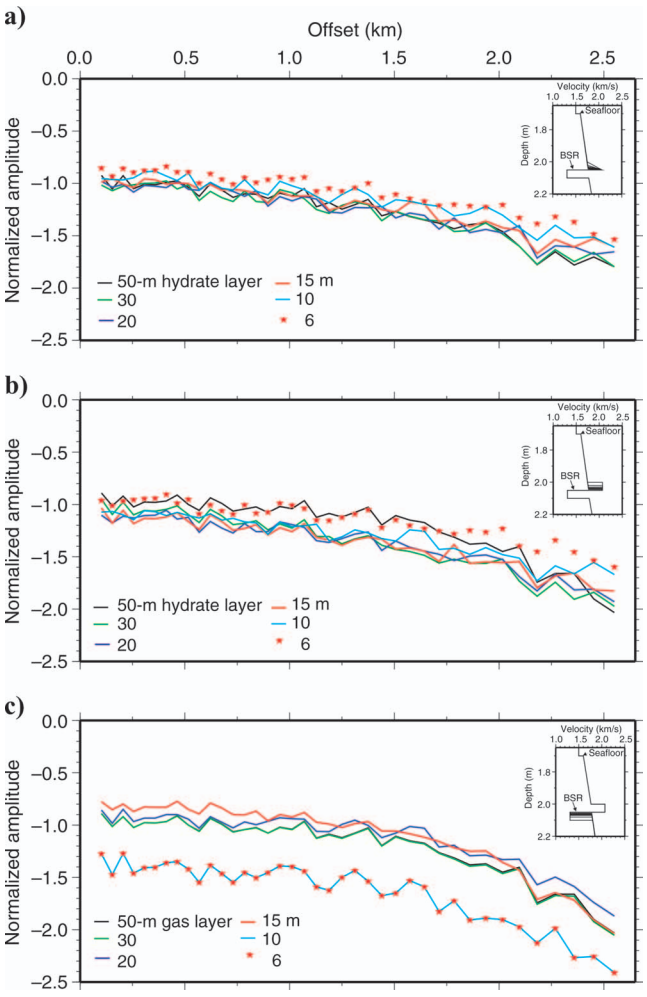

Figure 7. Modeled amplitudes of the BSR normalized with respect to the seafloor for several thicknesses of hydrate and free-gas layers (in sets). Velocity-depth functions are computed using BGTL theory for 20% hydrate and 2% gas with a *Q*-factor of 250 and 150 (Singh and Minshull, 1994), respectively. The synthetic seismograms are generated using the reflectivity method (Fuchs and Mueller, 1971) with the frequency band of 2–10–80–94 Hz. (a, b) Thick gas layers result in negligible tuning effects. However, considerable effects are observed (c) when the underlying gas layer is <10 m thick.

CONCLUSIONS

The *A*-*B* crossplot is a nomogram for various rock-physics models from which we can understand whether the BSR is underlain by gas and then directly estimate hydrate and gas content. The *A* and *B* values derived from the BSR in the Makran accretionary prism clearly deviate from the reference trend and thus indicate the presence of gas below the BSR. The EMT model indicates a hydrate saturation of 14–29% and a gas saturation of 1–6%, whereas the BGTL model indicates 4–15% hydrate and 1–7.5% gas, respectively, which varies laterally (Figure 6b). The AVO attribute analysis is simple and easy to implement across a wide area to estimate hydrate and gas saturations at a BSR.

ACKNOWLEDGMENTS

We are grateful to the director of the National Geophysical Research Institute (NGRI), India, for his kind consent to publish this work. The Ministry of Earth Sciences and the Department of Science and Technology, New Delhi, are acknowledged for their financial support. The associate editor and three anonymous reviewers are thanked for their useful comments and suggestions.

REFERENCES

Andreassen, K., P. E. Hart, and M. Mary, 1997, Amplitude versus offset modeling of the bottom simulating reflection associated with submarine gas hydrates: Marine Geology, **137**, 25–40.
Andreassen, K., K. Hogstad, and K. A. Berteussen, 1990, Gas hydrate in the southern Barents Sea indicated by a shallow seismic anomaly: First Break, **8**, 235–245.
Batzle, W., and Z. Wang, 1992, Seismic properties of pore fluids: Geophysics, **57**, 1396–1408.
Carcione, J. M., and U. Tinivella, 2000, Bottom-simulating reflectors: Seismic velocities and AVO effects: Geophysics, **65**, 54–67.
Castagna, J. P., and M. M. Backus, 1993, Offset dependent reflectivity: Theory and practice of AVO analysis: SEG.
Castagna, J. P., and S. W. Smith, 1994, Comparison of AVO indicators: A modeling study: Geophysics, **59**, 1849–1855.
Castagna, J. P., H. W. Swan, and D. J. Foster, 1998, Framework for AVO gradient and intercept interpretation: Geophysics, **63**, 948–956.
Chand, S., T. A. Minshull, D. Gei, and J. M. Carcione, 2004, Elastic velocity models for gas-hydrate bearing sediments — A comparison: Geophysical Journal International, **159**, 573–590.
Chapman, N. R., J. F. Gettrust, R. Walia, D. Hannay, G. D. Spence, W. T. Wood, and R. D. Hyndman, 2002, High-resolution, deep-towed, multichannel seismic survey of deep-sea gas hydrates off western Canada: Geophysics, **67**, 1038–1047.
Chen, M. P., M. Riedel, R. D. Hyndman, and S. E. Dosso, 2007, AVO inversion of BSRs in marine gas hydrate studies: Geophysics, **72**, no. 2, C31–C43.
Collett, T., M. Riedel, J. Cochran, R. Boswell, J. Presley, P. Kumar, A. Sathe, A. Sethi, M. Lall, V. Sibal, and the National Gas Hydrate Program (NGHP) Expedition 01 Scientists, 2008, Indian NGHP Expedition 01 initial reports: Directorate General Hydrocarbon report.
Dai, J., H. Xu, F. Snyder, and N. Dutta, 2004, Detection and estimation of gas hydrates using rock physics and seismic inversion: Examples from the northern deepwater Gulf of Mexico: The Leading Edge, **23**, 60–66.
Dillon, W. P., J. S. Booth, C. K. Paul, K. Fehlhaber, D. R. Hutchinson, and B. A. Swift, 1991, Mapping sub-seafloor reservoirs of a greenhouse gas: Methane hydrate: International Symposium on Marine Positioning, Marine Technology Society, Proceedings, 545–554.
Dvorkin, J., D. Moos, J. L. Packwood, and A. Nur, 1999, Identifying patchy saturation from well logs: Geophysics, **64**, 1759–1759.
Dvorkin, J., and A. Nur, 1996, Elasticity of high-porosity sandstones: Theory for two North Sea data sets: Geophysics, **61**, 1363–1370.
Ecker, C., J. Dvorkin, and A. Nur, 1998, Sediments with gas hydrates, Internal structure from seismic AVO: Geophysics, **63**, 1659–1669.
Fowler, S. R., R. S. White, and K. E. Louden, 1985, Sediment dewatering in the Makran accretionary prism: Earth and Planetary Science Letters, **75**, 427–438.
Fuchs, K., and G. Muller, 1971, Computation of synthetic seismograms with

the reflectivity method and comparison with observations: Geophysical Journal of the Royal Astronomical Society, **23**, 417–433.
Ghosh, R., and K. Sain, 2008, Effective medium modeling to assess gas hydrate and free-gas evident from the velocity structure in the Makran accretionary prism, offshore Pakistan: Marine Geophysical Research, **29**, 267–274.
Helgerud, M., J. Dvorkin, A. Nur, A. Sakai, and T. Collett, 1999, Elastic-wave velocity in marine sediments with gas hydrates: Effective medium modeling: Geophysical Research Letters, **26**, 2021–2024.
Hyndman, R. D., and G. D. Spence, 1992, A seismic study of methane hydrate marine bottom simulating reflectors: Journal of Geophysical Research, **97**, 6683–6698.
Kvenvolden, K. A., 1998, A primer on the geological occurrence of gas hydrate, *in* J. P. Henriet, and J. Mienert, eds., Gas hydrates: Relevance to the world margin stability and climate change: Geological Society, London, Special Publications, 137, 9–30.
Kvenvolden, K. A., G. D. Ginsburgh, and V. A. Soloviev, 1993, Worldwide distribution of subaquatic gas hydrates: Geo-Marine Letters, **13**, 32–40.
Lee, M. W., 2002, Biot-Gassmann theory for velocities of gas-hydrate bearing sediments: Geophysics, **67**, 1711–1719.
——–, 2004, Elastic velocities of partially gas-saturated unconsolidated sediments: Marine and Petroleum Geology, **21**, 641–650.
Lee, M. W., D. R. Hutchinson, T. S. Collett, and W. P. Dillon, 1996, Seismic velocities for hydrate-bearing sediments using weighted equation: Journal of Geophysical Research, **101**, 20347–20358.
Makogon, Y. F., S. A. Holditch, and T. Y. Makogon, 2007, Natural gas hydrates — A potential energy source for the 21st Century: Journal of Petroleum Science and Engineering, **56**, 14–31.
Malinverno, A., M. Kastner, M. E. Torres, and U. G. Wortmann, 2008, Gas hydrate occurrence from pore water chlorinity and downhole logs in a transect across the northern Cascadia margin (IODP Expedition 311): Journal of Geophysical Research, **113**, B08103.
Milkov, A. V., 2004, Global estimates of hydrate-bound gas in marine sediments, How much is really out there?: Earth Science Review, **66**, 183–197.
Minshull, T. A., and R. S. White, 1989, Sediment compaction and fluid migration in the Makran accretionary prism: Journal of Geophysical Research, **94**, 7387–7402.
Minshull, T. A., R. S. White, P. J. Barton, and J. S. Collier, 1992, Deformation at plate boundaries around the Gulf of Oman: Marine Geology, **104**, 265–277.
Ojha, M., and K. Sain, 2008, Appraisal of gas-hydrates/free-gas from V_P/V_S ratio in the Makran accretionary prism: Marine and Petroleum Geology, **25**, 637–644.
Ostrander, W. J., 1984, Plane-wave reflection coefficients for gas sands at non-normal angles of incidence: Geophysics, **49**, 1637–1649.
Paull, C. K., and W. P. Dillon, 2001, Natural gas hydrates, Occurrence, distribution, and detection: American Geophysical Union.
Paull, C. K., W. Ussler III, and W. P. Dillon, 1991, Is the extent of glaciation limited by marine gas-hydrates?: Geophysical Research Letters, **18**, 432–434.
Riedel, M., E. C. Willoughby, M. A. Chen, T. He, I. Novosel, K. Schwalenberg, R. D. Hyndman, G. D. Spence, N. R. Chapman, and R. N. Edwards, 2006, Gas hydrate on the northern Cascadia margin, Regional geophysics and structural framework: Proceedings of Integrated Ocean Drilling Program (IODP) 311, 1–28.
Ruppel, C., and M. Kinoshita, 2000, Fluid, methane, and energy flux in an active margin gas hydrate province, offshore Costa Rica: Earth and Planetary Science Letters, **179**, 153–165.
Sain, K., T. A. Minshull, S. C. Singh, and R. W. Hobbs, 2000, Evidence for a thick free-gas layer beneath the bottom simulating reflector in the Makran accretionary prism: Marine Geology, **164**, 3–12.
Sheriff, R. E., and L. P. Geldert, 1995, Exploration seismology — History, theory, data acquisition, vol. 1: Cambridge University Press.
Shuey, R. T., 1985, A simplification of Zoeppritz equations: Geophysics, **50**, 609–614.
Singh, S. C., and T. A. Minshull, 1994, Velocity structure of a gas hydrate reflector at Ocean Drilling Program site 889 from a global seismic waveform inversion: Journal of Geophysical Research, **99**, 24221–24233.
Sloan, E. D., 1998, Clathrate hydrate of natural gases: Marcel Deckker, Inc.
Taylor, C. E., and J. T. Kwan, 2004, Advances in the study of gas-hydrates: Kluwer Academic/Plenum Publishers.
Tinivella, U., 2002, The seismic response to overpressure versus gas hydrate and free gas concentration: Journal of Seismic Exploration, **11**, 283–305.
Trehu, A. M., P. E. Long, M. E. Torres, G. Bohrmann, F. R. Rack, T. S. Collett, D. S. Goldberg, A. V. Milkov, M. Riedel, P. Schultheiss, N. L. Bangs, S. R. Barr, W. S. Borowski, G. E. Claypool, M. E. Delwiche, G. R. Dickens, E. Garcia, G. Guerin, M. Holland, J. E. Johnson, Y. J. Lee, C. S. Liu, X. Su, B. Teichert, H. Tomaru, M. Vanneste, M. Watanabe, and J. L. Weinberger, 2004, Three-dimensional distribution of gas hydrate beneath the Southern Hydrate Ridge: Constraints from ODP leg 204: Earth and Planetary Science Letters, **222**, 845–862.
Warner, M., 1990, Absolute reflections from deep seismic reflections: Tectonophysics, **173**, 15–23.
White, J. E., 1975, Computed seismic speeds and attenuation in rocks with partial gas saturation: Geophysics, **40**, 224–232.
Wood, A. B., 1941, A textbook of sound: Macmillan Publ. Co.
Wyllie, M. R. J., A. R. Gregory, and G. H. F. Gardner, 1958, An experimental investigation of factors affecting elastic wave velocities in porous media: Geophysics, **23**, 459–493.
Yu, G., 1985, Offset-amplitude variation and controlled-amplitude processing: Geophysics, **50**, 2697–2708.
Yuan, T., G. D. Spence, R. D. Hyndman, T. A. Minshull, and S. C. Singh, 1999, Seismic velocity studies of a gas hydrate bottom-simulating reflector on the northern Cascadia continental margin, Amplitude modeling and full waveform inversion: Journal of Geophysical Research, **104**, 1179–1191.